

Critical study on P- and S-waves radiation and computation of earthquake magnitude due to simple crack models

Ajit De

Department of Mathematics, Siliguri College, Siliguri-734001, India
Email: ajit_math@rediffmail.com

ABSTRACT

The seismic radiation due to a dynamic crack model has been obtained in frequency domain by considering integral transformed displacement field in an infinite medium. The far field seismic spectra of P- and S-wave arrivals have been computed for the model. Study has also been extended in case of static elliptical shear crack model. Constant far-field displacement spectra have been observed at low frequencies and decay as some power of inverse frequency at high frequencies. Earthquake magnitude or Richter magnitude due to the source model has been computed and a comparative study of different magnitude scales has been presented. The special character of the source model has been compared and discussed with spectral scaling law.

Key words: Earthquake, Seismic radiation, Crack, Fourier transform, Richter magnitude.

INTRODUCTION

The radiation due to dislocation or crack models is useful in the study of deformation due to earthquakes. The radiation from simple source model has been obtained here in frequency domain by taking Fourier transformation. The total moment of any seismic source can also be obtained as low frequency limit of transformed time domain displacement field. It has been observed that individual earthquake is different from each other and can be modeled with different spectral scaling law. In the present study, far field seismic spectra at the body wave arrivals have been computed for both static and dynamic crack models with spectral behavior of the source time function. The spectral scaling law for the models has also been represented. An effort has also been made to compute the possible amplitude or earthquake magnitude for the source model and a comparative study of different magnitude scales has also been presented.

Earthquake source theories forecast a constant far-field displacement spectrum at low frequencies and the spectrum is inversely proportional to some power of frequency (ω) at high frequencies (Molnar et al., 1973; Brune, 1970). The near field signals radiated by earthquakes may become quite complex due to scattering, multipathing etc. and hence the actually observed seismogram resembles the source time function only at long periods (Madariaga, 2007). In general, the seismic spectra are of different types. It has been observed that spectra decay approximately as inverse square of the frequency (ω) at high frequencies (Aki, 1967; Brune, 1970) and the sources are described by seismic moment and corner frequency. But the spectrum of a trapezoidal source-time function is proportional to seismic moment (M_0) at low frequencies, a ω^{-1} segment at intermediate frequencies and a ω^{-2} fall off at high frequencies (Shearer,

2009). Earthquake size can be quantified by seismic moment (M_0) as it is directly related to the fundamental physical property of the source and various magnitude scales can be represented as functions of seismic moment. It is to be noted that the different earthquake measurement scales (M_L , m_b and M_S) exhibit large scatter among individual events of same moment and this may be due to variations in stress drop or other source properties or regional variations (Shearer, 2009).

Lancieri et al., (2012) studied the spectral scaling properties of a set of 68 aftershocks of the 2007 November 14 Tocopilla earthquake in north Chile under the assumption that the aftershocks satisfy an inverse omega-square spectral decay model. The aftershocks of Tocopilla earthquake are self-similar and are supported by Aki scaling law of seismic spectrum with the property of invariance of the apparent stress drop with earthquake size and invariance of a non-dimensional constant with the event size. Prieto et al., (2004) studied the scaling relationships of source parameters and self-similarity of earthquake spectra by analyzing 400 small earthquakes and observed that the ratio between radiated seismic energy and seismic moment is nearly constant and the corner frequencies vary inversely as the cube root of seismic moment.

The advantage of the present study is that it can be used to predict a suitable source model of an earthquake event and also the possible spectral amplitude due to some given seismic moment of the event.

FORMULATION AND CALCULATION OF THE SEISMIC SPECTRA

The present study has been extended to tackle two types of source models – Dynamic and Static.

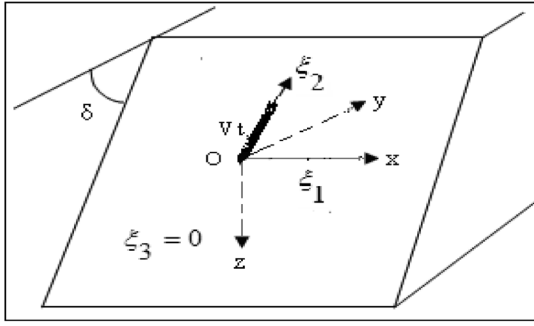


Figure 1. Dynamic Crack model under constant shear traction with two coordinate systems.

Case A: Dynamic Model

Effort has been made to reproduce far-field radiation and predict high frequency radiation by analyzing a two dimensional dynamic shear crack model as was proposed earlier by the author (De, 2014). The shear crack nucleates at a depth below the surface and propagates towards the surface with constant velocity V ($<$ shear wave velocity β) and under the influence of stress drop across the fault plane (De, 2014). The source has been considered as a time dependent dislocation and it acts as trigger for an earthquake with the bounding surface $z = -h$ in the half-space being free. The results in the study have been obtained in an infinite medium and in frequency domain via body force equivalent (De, 2014; Roy, 1979).

The displacement field due to a two dimensional dynamic crack [Figure 1] under constant shear traction acting on an inclined plane of arbitrary dip, can be evaluated following the author's earlier paper (De, (2014)). The displacement field at the outer edge P-wave arrival can be obtained from a similar expression as given in equation (4.13) of the author's paper (De, (2014)), but in an infinite medium by taking limit dimensionless time $\tau \rightarrow \frac{\beta}{\alpha} + 0$. The corresponding spectrum is given by

$$u_r(\omega) \approx \text{Re} \left[-\frac{1}{4\sqrt{2}(1+i)\pi R^*} \left(\frac{V}{\omega}\right)^{3/2} \frac{\mu\pi}{\alpha} A \exp[-i\omega(\beta/\alpha)] \right. \\ \left. \times \exp\left[-\frac{3}{2} \tanh^{-1}\left(\frac{RV}{\beta\omega} \{\cos\delta\eta - i\sin\delta(\eta^2+1)^{1/2}\}\right)\right] \eta \langle \eta e_r + i(\eta^2+1)^{1/2} e_z \rangle \frac{\partial \eta_p}{\partial \tau} \right] (2.1) \\ \left[\left(\frac{RV}{\beta} \{\cos\delta\eta - i\sin\delta(\eta^2+1)^{1/2}\}\right)^2 - \omega^2 \right]^{1/4}$$

where R^* is the epicentral distance, dimensionless time $\tau = \frac{\beta t}{R^*}$ and ω , the angular frequency.

The spectrum corresponding to S-wave arrival as dimensionless time $\tau \rightarrow 1 + 0$ is given by

$$u_s(\omega) \approx \text{Re} \left[-\frac{1}{4\sqrt{2}(1+i)\pi R^*} \left(\frac{V}{\omega}\right)^{3/2} \frac{\mu\pi}{\alpha} A \exp[-i\omega] \right. \\ \left. \times \exp\left[-\frac{3}{2} \tanh^{-1}\left(\frac{RV}{\beta\omega} \{\cos\delta\eta - i\sin\delta(\eta^2 + \frac{\alpha^2}{\beta^2})^{1/2}\}\right)\right] \frac{(2\eta^2 + \frac{\alpha^2}{\beta^2})}{\eta} \langle \eta e_r + i \frac{\eta^2}{(\eta^2 + \frac{\alpha^2}{\beta^2})^{1/2}} e_z \rangle \frac{\partial \eta_s}{\partial \tau} \right] (2.2) \\ \left[\left(\frac{RV}{\beta} \{\cos\delta\eta - i\sin\delta(\eta^2 + \frac{\alpha^2}{\beta^2})^{1/2}\}\right)^2 - \omega^2 \right]^{1/4}$$

The condition at the plane of crack surface $\zeta_3 = 0$:

$$\tau_{32} = \tau_0 + \tau_1 \zeta_2 ; \quad 0 < \zeta_2 < Vt,$$

$$\tau_{33} = 0$$

$$u_1 = u_2 \text{ for } \zeta_2 \notin (0, Vt) \text{ and } \tau_0, \tau_1 = \text{constants.}$$

The spectral behavior of the source time function is of the order $\omega^{-3/2}$, moderate than Brune's inverse omega-squared decay model (Brune, 1970). The corner frequency for the self-similar expanding crack model can be obtained as a spectrum's corner frequency where the high and low frequency trends intersect.

Case B: Static Model

Study has also been extended to a buried elliptic static shear crack model along an inclined fault plane with the bounding surface $z = -h$ in a half-space being free.

The displacement field at the outer edge P-wave arrival due to a static elliptic shear crack model [Figure 2] can be expressed as dimensionless time $\tau \rightarrow \frac{\beta}{\alpha} + 0$ [Appendix -A],

$$\vec{u}_r(\tau) \approx \frac{\alpha}{\beta} abH\left(\tau - \frac{\beta}{\alpha}\right) \text{Re} \left[\frac{\sqrt{2}\beta}{4\pi R_2 \alpha^2 S_2^{1/2}} \frac{8b(1-\nu)P}{\pi} A \frac{-\partial K_{p_2}}{\partial \tau} \Big|_{k_{p_2} = \frac{S_2}{R_2}} \right. \\ \left. \left\{ \left(\tau - \frac{\beta}{\alpha}\right)^{3/2} \left(\frac{\alpha}{\beta}\right)^{3/2} \vec{M}_{p_1}\left(i\frac{S_2}{R_2}\right) + 2i\left(\tau - \frac{\beta}{\alpha}\right)^{3/2} \left(\frac{\alpha}{\beta}\right)^{1/2} \vec{M}_{p_2}\left(i\frac{S_2}{R_2}\right) \right\} \right] \chi = \chi^* (2.3)$$

or equivalently, $\vec{u}_r(\tau) \approx M_0 H\left(\tau - \frac{\beta}{\alpha}\right) \text{Re} \left[\frac{\sqrt{2}\beta}{\pi^2 R_2 \alpha^2 S_2^{1/2}} A \frac{-\partial K_{p_2}}{\partial \tau} \Big|_{k_{p_2} = \frac{S_2}{R_2}} \right. \\ \left. \left\{ \left(\tau - \frac{\beta}{\alpha}\right)^{5/2} \left(\frac{\alpha}{\beta}\right)^{3/2} \vec{M}_{p_1}\left(i\frac{S_2}{R_2}\right) + 2i\left(\tau - \frac{\beta}{\alpha}\right)^{3/2} \left(\frac{\alpha}{\beta}\right)^{1/2} \vec{M}_{p_2}\left(i\frac{S_2}{R_2}\right) \right\} \right] \chi = \chi^* (2.4)$

where \bar{A} is some constant and ν is the Poisson's ratio.

The substitutions used in the above equation are

$$\xi = K \cos \chi, \quad \eta_p = K \sin \chi \quad \&$$

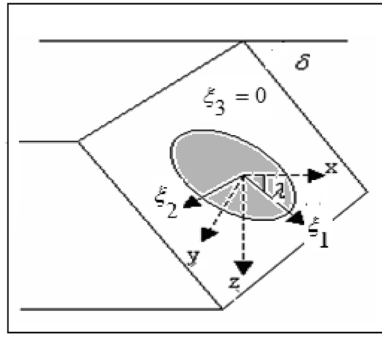
$$x = r \cos \theta, \quad y = r \sin \theta.$$

Thus the corresponding amplitude of the spectrum is given by,

$$u_r(\omega) \approx M_0 \text{Re} \left[-\frac{1}{\omega^{5/2}} \frac{2(1+i)}{\pi^2 R_2 \alpha} \left(\frac{\beta}{S_2 \alpha}\right)^{1/2} \Gamma(5/2) e^{-i\omega(\beta/\alpha)} \right] \chi = \chi^* (2.5)$$

and similarly for S-wave,

$$u_s(\omega) \approx M_0 A'' \text{Re} \left[-\frac{1}{\omega^{5/2}} \frac{2(1+i)}{\pi^2 R_2 \alpha} \left(\frac{\beta}{S_2 \alpha}\right)^{1/2} \Gamma(5/2) e^{-i\omega} \right] \chi = \chi^* (2.6)$$



The constant in-plane shear loading on the crack surface $\xi_3 = 0$

$$\tau_{\xi_1 \xi_3} = -PH \left(1 - \sqrt{\frac{\xi_1^2}{a^2} + \frac{\xi_2^2}{b^2}}\right) \delta(t) \delta(\xi_3)$$

$$\tau_{\xi_2 \xi_3} = -PH \left(1 - \sqrt{\frac{\xi_1^2}{a^2} + \frac{\xi_2^2}{b^2}}\right) \delta(t) \delta(\xi_3)$$

$$\tau_{\xi_3 \xi_3} = 0 \quad \forall (\xi_1, \xi_2, \xi_3) \in S$$

Figure 2. Elliptic Shear Crack model with two coordinate systems

where

$$S_2 = \{r(\cos \chi \cos \theta + \sin \chi \sin \theta \cos \delta) + h \sin \chi \sin \delta - \sqrt{a^2 \cos^2(\chi - \lambda) + b^2 \sin^2(\chi - \lambda)}\}$$

$R_2 = \sqrt{S_2^2 + (h \cos \delta - r \sin \theta \sin \delta)^2}$ is minimum at $\chi = \chi^*$ and M_0 = Scalar Seismic Moment of the crack model (Aki, 1966; Kelis-Borok, 1959)

= μ [Area of the elliptic crack face] [1- ν Maximum final dislocation for 100% stress drop]

= $\mu(\pi ab) \frac{3}{4} \left(\frac{\alpha}{\beta} \frac{2b}{\mu\pi} P\right)$ [Poisson's ratio $\nu = 0.25$, for the present case]

= $\frac{18}{7} ab^2 P$ [where $\frac{\alpha}{\beta} \approx \sqrt{3} \approx \frac{12}{7}$, for the present case] (2.7) where P is the uniform stress drop over the fault zone.

Thus, the Scalar Seismic Moment for the elliptic crack model is proportional to the cube of the linear dimension of the model and it may be predicted that the scalar seismic moment M_0 grows as the cube of the linear size of earthquake. The corresponding spectral behavior of the source time function is of the order $\omega^{-5/2}$, steeper than Brune's (1970) inverse omega-squared decay model.

DISCUSSION

The spectra [Eqns. (2.1) & (2.2)] for the dynamic crack model under constant shear traction decay with frequency at least as fast as $\omega^{-3/2}$ at frequencies higher than the corner frequency (De, (2014)). It is clear from Figure 3 that the corner frequency for P-wave spectra due to a two dimensional dynamic crack model moving with rupture velocity more than the shear wave velocity, decreases with the inclination of the fault plane. Similar phenomenon with slight variation of corner frequency is observed for rupture velocity equal to that of shear velocity (Figure 4). It is clear from the equations (2.1) and (2.2) that the shape of the spectra for the model are determined by the parameters $\frac{VR}{\beta} \{\cos \delta \eta - i \sin \delta (\eta^2 + 1)^{1/2}\}$ and $\frac{VR}{\beta} \{\cos \delta \eta - i \sin \delta (\eta^2 + \frac{\alpha^2}{\beta^2})^{1/2}\}$; respectively for P and S waves and can be used to determine the corner frequencies of the respective spectrum. Figure 5 shows that P-wave corner frequency exceeds S-wave corner frequency for the dynamic crack model and spectra are nearly alike for different rupture velocities. The P- and S-wave corner frequency ratio for the model is very near to

one. Our result resembles with the observation of Savage, (1974) and Molnar et al., (1973).

Seismic moment is a key observable parameter related to an earthquake. It is a static measure of earthquake size and quantitative measure related to the amount of earth movement during the event. It is also independent of rupture time history. The elliptic crack model as discussed in equation (2.3) or (2.4) may fit as a better approximation of seismic rupture process than Haskell's dislocation model (Haskell, 1964; Haskell, 1966) and the seismic spectra as presented in equations (2.5) and (2.6) decay as $\omega^{-5/2}$ at high frequencies (Figure 6).

In previous work referring to the computation of theoretical seismogram model due a two dimensional dynamic crack (De, 2014, Figure 2) shows that maximum dimensionless amplitude is 0.112 at the dimensionless time 1.0. We consider the parameters of the study as

$$r = y = 50 \text{ km}, \beta = 3.5 \text{ km/s}, \rho = 2.8 \text{ gm/cm}^3, \mu = 3.43 \text{ MPa}, \tau_0 = 10 \text{ MPa}, \pi = 3.14.$$

Now taking the approximate empirical formula for the computation of local (Richter) magnitude, M_L (Bullen and Bolt, 1985)

$$M_L = \log_{10} A + 2.56 \log_{10} D - 1.67 \quad (3.1)$$

where A is the measured maximum ground displacement amplitude in micrometers (at the S-wave arrival) and $D = r$ is the distance from the event (in km), the computed local magnitude M_L is 6.0.

[The computed amplitude for the present case

$$A = \frac{3\tau_0}{\mu\pi^2 r} 0.11 = 1949.62]$$

The local (Richter) magnitude scale is used to measure shallow earthquake events of magnitude less than 6.5 and is used complimentary to other magnitude scales like, Body wave Magnitude (m_b) and Surface wave magnitude (M_s). In the present days the moment magnitude scale (M_w) is used for effective computation of large earthquake events and with the respective formula for its computation is (as defined in Aki and Richards, 2002)

$$M_w = \frac{2}{3} [\log_{10} M_0 - 9.1] \quad (3.2)$$

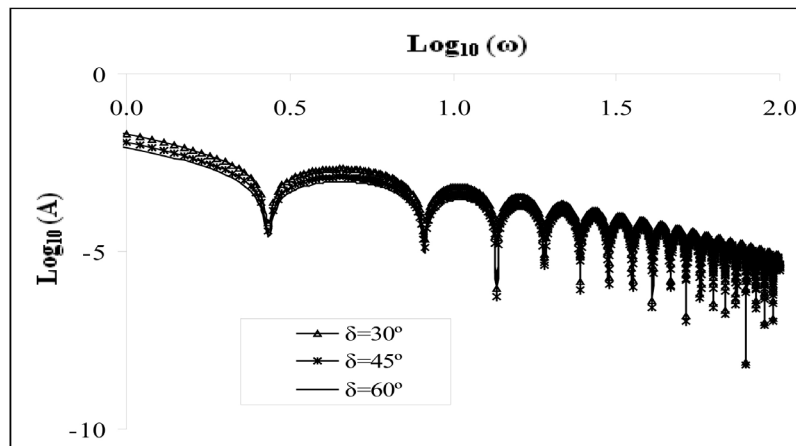


Figure 3. Dimensionless spectra (A) – frequency (ω) graph at an epicentral distance 100 km. (in y-z plane) due to a two dimensional dynamic shear crack model moving with velocity greater than that of shear wave (i.e., $V > \beta$) at the P-wave arrival for different dip angles (δ).

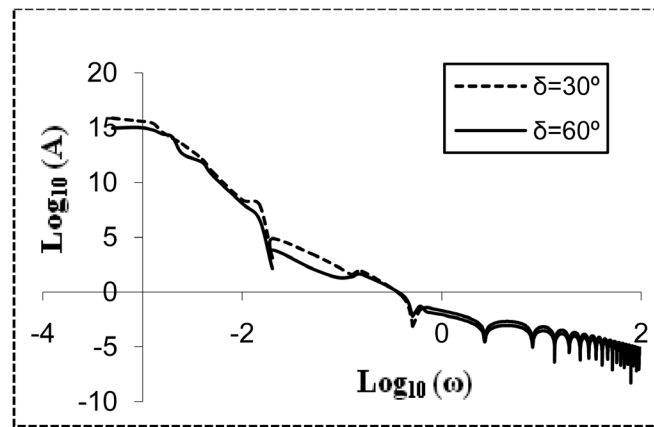


Figure 4. Dimensionless spectra (A) – frequency (ω) graph at an epicentral distance 100 km. (in y-z plane) due to a two dimensional dynamic shear crack model moving with velocity equal to that of shear wave (i.e., $V = \beta$) at the P-wave arrival for different dip angles (δ).

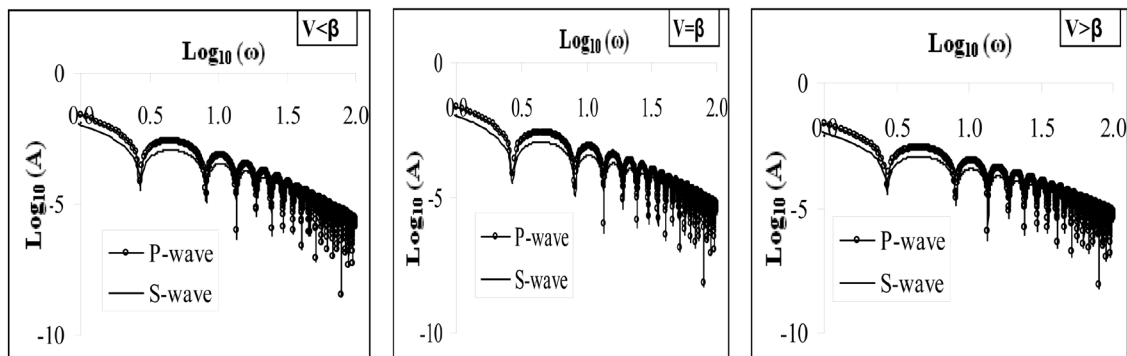


Figure 5. Comparison of dimensionless spectra (A) at the arrivals of P- and S-waves against dimensionless frequency (ω) at an epicentral distance 50 km. (in y-z plane) due to a dynamic two dimensional shear crack model moving with different rupture velocity at the dip angle $\delta = 60^\circ$.

Where, M_0 is the seismic moment in N-m. Local magnitude scale $M_L \approx M_w$ (Prieto et. al., 2004) and the present study establish the fact (Table 1 & 2). The present study also

reveals that the maximum predicted amplitude at a place decreases with the increasing values of dip angle and increase in stress drop increases the predicted amplitude

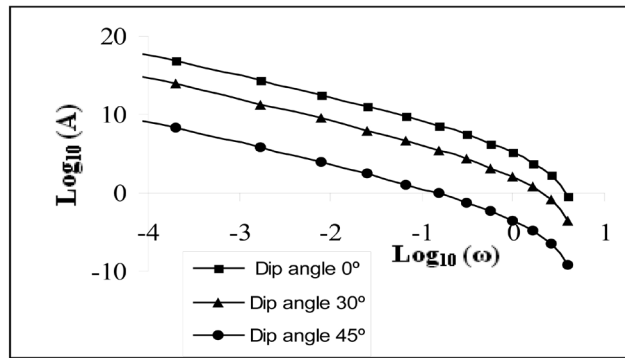


Figure 6. Dimensionless spectra (A) – frequency (ω) graph at an epicentral distance 100 km due to a static elliptic in-plane crack model with semi-axis ratio $a/b = 2$.

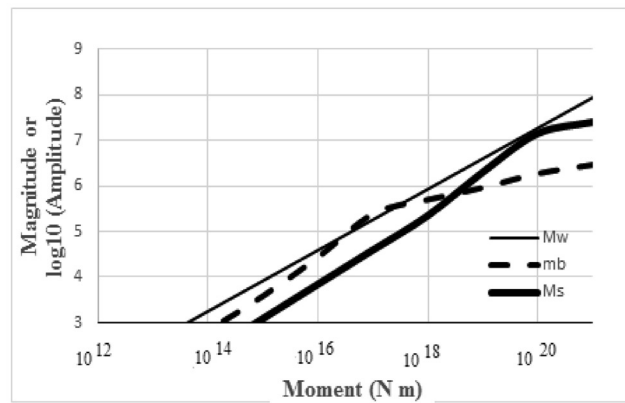


Figure 7. Different magnitude scales (M_w , m_b and M_s) or predicted \log_{10} (Amplitude) for the $\omega^{-3/2}$ shear moving crack model have been presented here as functions of seismic moment (M_0). The crack is moving with a velocity $(9/10)$ times that of shear wave (β) velocity and a constant stress drop of 3 MPa has been assumed. Approximately, the amplitude is proportional to M_0 initially, $M_0^{2/3}$ intermediate stage and finally $M_0^{1/3}$.

Table 1. Comparative study on different magnitude scales at a place (epicentral distance 50 Km.) for different source parameters of the dynamic crack model.

Sl. No.	Rupture velocity (V)	Stress Drop on the fault plane	Dip angle of the fault plane (δ)	Maximum Amplitude (Micrometer)	Seismic Moment (M_0) (N-m)	M_w	M_L
1.	V=0.9 β	3 MPa	30°	595.04	3×10^{17}	5.6	5.4
2.			60°	478.16			5.4
3.		6 MPa	30°	1190.08	6×10^{17}	5.8	5.8
4.			60°	956.32			5.7
5.	V=1.2 β	3 MPa	30°	691.93	4×10^{17}	5.7	5.5

Table 2. Comparative study on different magnitude scales at a place (epicentral distance 50 Km.) For different source parameters of the static crack model with semi-axis ratio $a/b = 2$.

Sl. No.	Stress Drop on the fault plane	Dip angle of the fault plane (δ)	Maximum Amplitude (Micrometer)	Seismic Moment (M_0) (N-m)	M_w	M_L
1.	3 MPa	30°	598.60	4.2×10^{17}	5.7	5.5
2.		60°	528.32			5.4
3.	6 MPa	30°	1265.31	8.4×10^{17}	5.9	5.8
4.		60°	927.10			5.6

and seismic moment at a place considerably (Table 1 & 2). The Table 1 shows a comparative study at different rupture velocities of the dynamic crack model and predicts increasing amplitude and earthquake magnitude at higher rupture velocity. Figure 6 shows that \log_{10} (Dimensionless amplitude) = 14.2 (for $\delta = 30^\circ$) at low frequency (ω) limit (i.e., $\omega \rightarrow 0$) and this can be used to compute the seismic moment of the event. The computation reveals that corresponding \log_{10} (amplitude) = $\log_{10} (M_0) = 17.62$ and $M_W = 5.7$. Again Figure 4 shows that \log_{10} (Dimensionless amplitude) = 15.8 (for $\delta = 30^\circ$) at low frequency limit and the corresponding \log_{10} (amplitude) = $\log_{10} (M_0) = 19.22$ and $M_W = 6.7$. Figure 7 shows the predicted amplitude for given seismic moment in different magnitude scales (M_w , m_b and M_S). The m_b approximates M_w upto the magnitude 5.5 and under predicts M_w above that value. But M_S agrees approximately with M_W between 6.6 to 7.3 and under predicts M_W outside the interval. The present study approximately agrees with the results of an ω^{-2} source model of Madariaga (Shearer, 2009) for an assumed constant stress drop of 3 MPa. If the stress drop be increased to another constant value, say 6 MPa and other conditions be kept fixed then the corresponding moment as well as predicted amplitude will rise comparatively. Similar study with slight variation is observed for the static model.

Appendix-A

Approximate displacement field near outer edge P-wave arrival due to the static shear crack model

The displacement field at the outer edge P-wave arrival can be expressed in an infinite medium as dimensionless time $\tau \rightarrow \frac{\beta}{\alpha} + 0$ (De, (2013); Roy, (1984)),

$$\vec{u}_p \approx \lim_{\varepsilon \rightarrow 0, \tau \rightarrow \frac{\beta}{\alpha} + 0} H\left(\tau - \frac{\beta}{\alpha}\right) \int_{\chi^* - \varepsilon}^{\chi^* + \varepsilon} \frac{2ab}{4i\pi R_2 \alpha^3} \frac{8b(1-\nu)P}{\pi} \frac{d\chi}{\chi^* - \varepsilon} \left[\left(\frac{\beta}{4R_2}\right) \frac{\partial K_{P_2}}{\partial \tau} \left\{ \left(\tau - \frac{\beta}{\alpha}\right)^2 i \left(\frac{\alpha}{\beta}\right)^2 \vec{M}_{P_1}(K_{P_2}) - 2\left(\frac{\alpha}{\beta}\right) \left(\tau - \frac{\beta}{\alpha}\right) \vec{M}_{P_2}(K_{P_2}) \right\} \right] d\chi \quad (A.1)$$

where \bar{A} is some constant.

Now evaluating the integral at $\tau = \frac{\beta}{\alpha}$ and proceeding to the limit $\varepsilon \rightarrow 0$,

$$\vec{u}_p \approx H\left(\tau - \frac{\beta}{\alpha}\right) \lim_{\varepsilon \rightarrow 0} \text{Re} \left[\frac{2\varepsilon\alpha ab}{2i\pi R_2 \alpha^3} \frac{8b(1-\nu)P}{\pi} \frac{\partial K_{P_2}}{\partial \tau} \left\{ \left(\tau - \frac{\beta}{\alpha}\right)^2 i \left(\frac{\alpha}{\beta}\right)^2 \vec{M}_{P_1}\left(i\frac{S_2}{R_2}\right) - 2\left(\frac{\alpha}{\beta}\right) \left(\tau - \frac{\beta}{\alpha}\right) \vec{M}_{P_2}\left(i\frac{S_2}{R_2}\right) \right\} \right] \chi = \chi^* \quad (A.2)$$

Again R_2 is minimum at $\chi = \chi^*$ and $R_1(\chi^* + \varepsilon) = R_1(\chi^*) + \frac{1}{2}\varepsilon^2 \frac{S_1}{R_1}$. Thus ε can be approximated as $\varepsilon = \frac{\sqrt{2R_1}}{S_1^{1/2}} \left(\frac{\alpha}{\beta}\right)^{1/2} \left(\tau - \frac{\beta}{\alpha}\right)^{1/2}$. Hence,

$$\vec{u}_p \approx \frac{\alpha}{\beta} abH\left(\tau - \frac{\beta}{\alpha}\right) \text{Re} \left[-\frac{\sqrt{2}\beta}{4\pi R_2 \alpha^3 S_1^{1/2}} \frac{8b(1-\nu)P}{\pi} \frac{\partial K_{P_2}}{\partial \tau} \right]_{K_{P_2} = \frac{S_2}{R_2}} \left\{ \left(\tau - \frac{\beta}{\alpha}\right)^{3/2} \left(\frac{\alpha}{\beta}\right)^{3/2} \vec{M}_{P_1}\left(i\frac{S_2}{R_2}\right) + 2i \left\{ \left(\tau - \frac{\beta}{\alpha}\right)^{1/2} \left(\frac{\alpha}{\beta}\right)^{1/2} \vec{M}_{P_2}\left(i\frac{S_2}{R_2}\right) \right\} \right\} \chi = \chi^* \quad (A.3)$$

where M_{P_j} (K_{P_j}) $\{j=1,2\}$ are functions of K_{P_j} (De, (2013)) and are given by

$$\vec{M}_{P_1}(K) = A^* \frac{\{2\zeta_s(\xi \hat{e}_x + \eta \hat{e}_y) + i(2\xi^2 + 2\eta^2 + \frac{\alpha^2}{\beta^2})\hat{e}_z\}}{2(K\sqrt{a^2 \cos^2(\chi - \lambda) + b^2 \sin^2(\chi - \lambda)})^3} \frac{(\xi^2 + \eta^2 + 1)^{1/2}}{(K^2 + 1)^{1/2}}$$

$$\vec{M}_{P_2}(K) = A^* \frac{\{2\zeta_s(\xi \hat{e}_x + \eta \hat{e}_y) + i(2\xi^2 + 2\eta^2 + \frac{\alpha^2}{\beta^2})\hat{e}_z\}}{2K^2(a^2 \cos^2(\chi - \lambda) + b^2 \sin^2(\chi - \lambda))} \frac{(\xi^2 + \eta^2 + 1)^{1/2}}{(K^2 + 1)^{1/2}}$$

$F(\xi, \eta)A^* = [(A_1 \cos \lambda - A_2 \sin \lambda)\xi \cos \delta + (A_1 \sin \lambda + A_2 \cos \lambda)\eta] (i-1)(\xi^2 + \eta^2 + 1)^{1/2}$
 $F(\xi, \eta) = (2\xi^2 + 2\eta^2 + (\alpha^2/\beta^2))^2 - 4(\xi^2 + \eta^2)(\xi^2 + \eta^2 + 1)^{1/2}(\xi^2 + \eta^2 + \alpha^2/\beta^2)^{1/2}$
 with the path of steepest descent or Cagniard path as

$$\alpha t = (K^2 + 1)^{1/2} (h \cos \delta - r \sin \theta \sin \delta) - iK [r(\cos \chi \cos \theta + \sin \chi \sin \theta \cos \delta) + h \sin \chi \sin \delta \pm \sqrt{a^2 \cos^2(\chi - \lambda) + b^2 \sin^2(\chi - \lambda)}]$$

ACKNOWLEDGMENT

The work was supported financially by U.G.C., New-Delhi, India under MRP (Sanction No. F PSW-200/15-16 (ERO)). The author is thankful to the referees Dr. Anastasia Kiratzi and Dr. S.N. Bhattacharya for critical evaluation and objective reviewing. Thanks are due to Prof. B.V.S. Murty for final refinement and the Chief Editor, JIGU for valuable suggestions and timely support.

Compliance with Ethical Standards:

The author declares that he has no conflict of interest and adheres to copyright norms.

REFERENCES

- Aki, K., 1967. Scaling law of seismic spectrum, J. Geophys. Res., v.72, pp: 1217-1231.
- Aki, K., 1966. Generation and propagation of G waves from the Niigata earthquake of June 16, 1964. Estimation of earthquake movement, released energy and stress-strain drop from G-wave spectrum, Bul. Earthquake Res. Inst., v.44, pp: 23-88.
- Aki, K. and Richards, P.G., 2002. Quantitative Seismology Second Edition, University Science Books, Sausalito, California.
- Brune, J.N., 1970. Tectonic stress and the spectra of seismic shear waves from Earthquakes, J. Geophys. Res., v.75, pp: 4997-5009.
- Bullen, K.E. and Bolt, B.A., 1985. An introduction to the theory of seismology, 4th ed., Cambridge University Press.

Critical study on P- and S-waves radiation and computation of earthquake magnitude due to simple crack models

- De, A., 2014. Two dimensional self-similar expanding crack problems in elastic half-space, *Wave Motion*, v.51, pp: 852-864.
- De, A., 2013. Computation of synthetic seismogram for a buried elliptic in plane shear dislocation model in an elastic half-space, *J. Indian Math. Soc.*, v.80, pp: 243-263.
- Haskell, N.A., 1966. Total energy spectral density of elastic wave radiation from propagating faults. Part-II. A statistical source model, *Bull. Seismol. Soc. Am.*, v.56, pp: 125-140.
- Haskell, N.A., 1964. Total energy spectral density of elastic wave radiation from propagating faults, *Bull. Seismol. Soc. Am.*, v.54, pp: 1811-1841.
- Keilis-Borok, V.I., 1959. On the estimation of the displacement in an earthquake source and of source dimensions, *Annales de Geophysique*, v.12, pp: 205-214.
- Lancieri, M., Madariaga, R. and Bonilla, F., 2012. Spectral scaling of the aftershocks of the Tocopilla 2007 earthquake in northern Chile, *Geophys.J. Int.*, v.189, no.1, pp: 469-480.
- Madariaga, R., 2007. Seismic source theory, in: Kanamori, H. (Ed.), *Earthquake Seismology*. in: *Treatise of Geophysics*, Academic Press, v.4, no.2, pp: 59-82.
- Molnar, P., Tucker, B.E. and Brune, J.N., 1973. Corner frequencies of P and S waves and models of earthquake sources, *Bull. Seismol. Soc. Am.*, v.63, no.6, pp: 2091-2104.
- Prieto, G.A., Shearer, P.M., Vernon, F.L. and Kilb, D., 2004. Earthquake source scaling and self-similarity estimation from stacking P and S spectra, *J. Geophys. Res.*, v.109, B08310, doi:10.1029/2004JB003084.
- Roy, A., 1984. Diffraction of elastic waves by an elliptic crack, *Int. J. Eng. Sci.*, v.22, pp: 729-735.
- Roy, A., 1979. On dislocations and extended sources in an elastic half-space, *Indian J. Pure Appl. Math.*, v.10. no.1, pp: 100 – 111.
- Savage, J.C., 1974. Relation between P- and S-wave corner frequencies in the seismic spectrum, *Bull. Seismol. Soc. Am.*, v.64, pp: 1621-1627.
- Shearer, Peter M., 2009. *Introduction to seismology*, Cambridge University Press, pp: 241-295.

Received on: 20.6.17; Revised on: 27.8.17; Re revised on: 16.10.17; Accepted on: 30.11.2017